The Journal of Immunology

Evolution and Potential Subfunctionalization of Duplicated *fms*-Related Class III Receptor Tyrosine Kinase *flt3*s and Their Ligands in the Allotetraploid *Xenopus laevis*

Matthieu Paiola, Siyuan Ma and Jacques Robert

J Immunol published online 5 August 2022
http://www.jimmunol.org/content/early/2022/08/12/jimmunol.2200201

Supplementary Material **http://www.jimmunol.org/content/suppl/2022/08/05/jimmunol.2200201.DCSupplemental**

The Journal of Immunology is published twice each month by
The American Association of Immunologists, Inc.,
1451 Rockville Pike, Suite 650, Rockville, MD 20852

Print ISSN: 0022-1767 Online ISSN: 1550-6606.

Published August 12, 2022, doi:10.4049/jimmunol.2200201

Evolution and Potential Subfunctionalization of Duplicated *fms*-Related Class III Receptor Tyrosine Kinase *flt3*s and Their Ligands in the Allotetraploid *Xenopus laevis*

Matthieu Paiola, Siyuan Ma, and Jacques Robert

The *fms*-related tyrosine kinase 3 (Flt3) and its ligand (Flt3lg) are important regulators of hematopoiesis and dendritic cell (DC) homeostasis with unsettled coevolution. Gene synteny and deduced amino acid sequence analyses identified conserved *flt3* gene orthologs across all jawed vertebrates. In contrast, *flt3lg* orthologs were not retrieved in ray-finned fish, and the gene locus exhibited more variability among species. Interestingly, duplicated *flt3/flt3lg* genes were maintained in the allotetraploid *Xenopus laevis*. Comparison of modeled structures of *X. laevis* Flt3 and Flt3lg homoeologs with the related diploid *Xenopus tropicalis* and with humans indicated a higher conformational divergence between the homoeologous pairs than their respective counterparts. The distinctive developmental and tissue expression patterns of Flt3 and Flt3lg homoeologs in tadpoles and adult frogs suggest a subfunctionalization of these homoeologs. To characterize Flt3 cell surface expression, *X. laevis*–tagged rFlt3lg.S and rFlt3lg.L were produced. Both rFlt3lg.S and rFlt3lg.L bind in vitro Flt3.S and Flt3.L and can trigger Erk1/2 signaling, which is consistent with a partial overlapping function between homoeologs. In spleen, Flt3.S/L cell surface expression was detected on a fraction of B cells and a population of MHC class II^{high}/CD8^{+} leukocytes phenotypically similar to the recently described dual follicular/conventional DC-like XL cells. Our result suggests that 1) Flt3lg.S and Flt3lg.L are both involved in XL cell homeostasis and that 2) XL cells have hematopoietic origin. Furthermore, we detected surface expression of the macrophage/monocyte marker Csf1r.S on XL cells as in mammalian and chicken DCs, which points to a common evolutionary origin in vertebrate DCs. *The Journal of Immunology*, 2022, 209: 1–10.

Bone marrow–derived dendritic cells (DCs) are central to the mammalian immune system by bridging the adaptive and innate arms. By processing and presenting Ags in the context of the MHC, DCs trigger T cell–mediated immune responses by interacting with the TCR. TCR signaling, leading to T cell activation, depends on various factors, including the affinity of the TCR for the Ag–MHC complex, the expression of coreceptors (CD4 and CD8), as well as costimulation (e.g., CD28) and coinhibition signals (e.g., CTLA-4 and PD-1) provided by their respective ligands (CD80/86 and PDL1) on APCs (1, 2). In secondary lymphoid organs, migratory conventional DCs (cDCs) drive adaptive immune responses and maintain systemic homeostasis against invading pathogens and harmless Ags, respectively (3). Adaptive immunity characterized by MHC molecules and somatically diversified Ag receptors of the Ig superfamily (TCRs and BCRs) is thought to having arisen in the common ancestor of all jawed vertebrates (4). Whereas B and T cells are easily identified by their respective receptors or coreceptors in all jawed vertebrates, the identification of DCs has been more challenging because of their numerous common features with macrophages (5). To date, dendritic-like cells have been mostly described in Gnathostomata according to their morphology, high expression of MHC class II (MHC-II), and costimulatory molecules (CD83, CD80) (5–7). Functionally, dendritic-like cells in ray-fined fish and birds have the capacity to phagocytose and, importantly, to stimulate T cell proliferation in vitro (5, 6, 8). In *Xenopus*, single DC-like cells called XL cells have been identifies in the spleen to date (9, 10). XL cell features are reminiscent of both mammalian follicular and conventional DCs, because they express a high level of MHC-II, bind and retain native Ags, express genes related to both follicular DCs (FDCs) and cDCs (*spi1*, *cxcl13*, and *ccl19*), and are in close contact to B and T cells (10). Therefore, it was hypothesized that XL cells represent a primordial "double-duty" DC with FDC and cDC roles in *Xenopus*, and likely in all ectotherms that lack bona fide FDCs. Although increasing evidence suggests that dendritic-like cells are present in all ectotherm vertebrates, many aspects of their ontogeny, physiology, and function are unknown.

The *fms*-related tyrosine kinase 3 (Flt3), also known as CD135, belongs to a family of the class III receptor tyrosine kinases (RTKs) that includes Kit (CD117), CSF1 receptor (Csf1r; CD115), and platelet-derived growth factor receptors (Pdgfrs). Similar to other RTKs, Flt3 is a cell surface receptor that binds its cognate extracellular Flt3 ligand (Flt3lg). The high-affinity ligand binding leads to receptor activation of the intracellular tyrosine kinase domain, which initiates multiple intracellular signaling cascades (11, 12). In humans and mice, Flt3 is expressed by hematopoietic, lymphoid, and DC progenitors in the bone marrow as well as by mature DCs in lymph nodes and spleen. As such, Flt3 signaling regulates progenitor survival and proliferation, as well as DC

Department of Microbiology and Immunology, University of Rochester Medical Center, Rochester, NY

ORCIDs: 0000-0002-3536-861X (M.P.); 0000-0001-5739-2568 (S.M.); 0000-0003-4380-1476 (J.R.).

Received for publication March 15, 2022. Accepted for publication June 29, 2022.

This work was supported by National Institute of Allergy and Infectious Diseases Grants R21AI139718 and R24AI059830 from National Science Foundation Grant IOS-1754274.

Address correspondence and reprint requests to Dr. Jacques Robert, Department of Microbiology and Immunology, University of Rochester Medical Center, Rochester, NY 14642. E-mail address: jacques_robert@urmc.rochester.edu

The online version of this article contains supplemental material.

Abbreviations used in this article: cDC, conventional DC; Csf1r, CSF1 receptor; DC, dendritic cell; FDC, follicular DC; Flt3, *fms*-related tyrosine kinase 3; Flt3lg, Flt3 ligand; L, long; MHC-II, MHC class II; MYA, million years ago; RTK, receptor tyrosine kinase; RT-qPCR, quantitative reverse transcription–PCR; S, short.

homeostasis (13, 14). Flt3 overexpression or mutation is associated with hematological cancers, including acute myeloid leukemia and B and T cell acute lymphoblastic leukemia (11, 13). Similar to Csf1r and Kit, Flt3 is evolutionarily conserved in jawed vertebrates, including teleost fish and tetrapods (15, 16). The Flt3 conserved role in hematopoiesis in zebrafish is supported by impairment of hematopoiesis induced by gene silencing with morpholinos, as well as expansion of the myeloid compartment resulting from the expression of a constitutively activated human FLT3 gene (16). In contrast, the role of Flt3 in DC biology outside mammals is less clear. Recently, *flt3* transcripts and Flt3 molecules have been detected in dendritic-like cells of the Atlantic cod and chicken, respectively, suggesting that Flt3 has an evolutionarily conserved role in DC development and homeostasis (8, 17–19).

In mammals, Flt3lg is required for DC differentiation and homeostasis (20–24). Hematopoietic growth factors such as Flt3lg are dimeric short-chain α-helical bundles (12). They are expressed as membrane forms at the cell surface and are secreted by proteolytic cleavage or alternative splicing (11). Both secreted and membrane forms are biologically active, although their potential distinct biological roles remain unclear (11). Flt3lg proteins are abundantly produced by various immune and nonimmune cells, including bone marrow, stromal cells (endothelial cells), T cells, and thymic fibroblasts (11, 25–28). Interestingly, unlike Csf1 and Kit ligand, which are conserved across most jawed vertebrates, Flt3lg gene orthologs have only been identified in tetrapods to date (29).

The evolution of immune genes in jawed vertebrates has been shaped by two rounds of whole-genome duplications, as well as by species-specific tandem gene duplications (30, 31). Duplicated genes often undergo negative selection by loss of function (pseudogenization or diploidization), which leads to singletons. Alternatively, gene duplication can trigger neo- or subfunctionalization (32). Such phenomena can provide a glimpse into functional evolution of complex immune factors such as Flt3lg/Flt3. Whereas *Xenopus tropicalis* is a diploid species, its relative *Xenopus laevis* is an allotetraploid species that arose by hybridization of two diploid species some 17–18 million years ago (MYA) (33). Interestingly, the two subgenomes evolved asymmetrically, with the short (S) chromosomes having undergone more interchromosomal rearrangements, gene losses, and silenced gene expression than the long (L) chromosomes (33). Notably, most genes involved in Ag receptor generation (e.g., TCR and BCR), Ag presentation (e.g., MHC class Ia and MHC-II), and complement and pathogen recognition have been lost in S homoeologous chromosomes, whereas multiple genes encoding proteins involved in costimulation (e.g., CD86), signaling (e.g., Lck), cytokines, and cytokine receptors have been retained presumably because of stoichiometrically controlled expression or subfunctionalization of the two homoeologous genes (32, 33). During our efforts to improve immune gene annotation in *Xenopus* genomes, we noted the occurrence of Flt3 and Flt3lg genes in the conserved genomic region of *X. laevis* L and S chromosomes. This motivated our interest to further investigate the expression profiles and functions of these homoeologous genes.

In the present work, we have investigated the evolution of Flt3/Flt3lg genes in gnathostomes. We found that although *flt3* is well conserved across all jawed vertebrates, *flt3lg* was only retrieved in tetrapods and cartilaginous and lobe-finned fish but not in ray-finned fish. Furthermore, we provide evidence that duplicated *X. laevis flt3* and *flt3lg* have been retained and likely subfunctionalized during evolution. Our study using recombinant tagged Csf1.S and Flt3lgs also substantiates the hematopoietic origin of XL cells suggesting a common origin of DCs in tetrapods.

Materials and Methods

Animals

Premetamorphic tadpoles (stage 56) and adult frogs (1 y old) were obtained from the *X. laevis* research resource for immunology at the University of Rochester (https://www.urmc.rochester.edu/microbiology-immunology/xenopus-laevis.aspx). Animals were handled in accordance with the stringent laboratory and University Committee on Animal Research regulations (approval no. 100577/2003-151).

Phylogenetic and gene synteny analysis

Deduced Flt3 and Flt3lg amino acid sequences were obtain using public databases (https://www.ncbi.nlm.nih.gov/, https://www.xenbase.org/) and were aligned using the MUSCLE algorithm. The length of the predicted Flt3lg is highly different across the investigated genera, and thus only the domains predicted as a 4-helix cytokine–like core were used for protein alignment. Domain prediction was carried out using the online server InterPro (https://www.ebi.ac.uk/interpro/). Full Flt3 sequences were used for multiple alignment and phylogenetic analysis. Phylogeny was inferred using the neighbor-joining method (34) using MEGA X (35, 36). Confidence of branching was estimated by percent bootstrapping (1000 replicates).

Structure comparison

Predicted functional domains of Flt3/Flt3lg from the *X. laevis* S and L chromosomes, *X. tropicalis*, and *Homo sapiens* were aligned using the online platform (http://multalin.toulouse.inra.fr/) (37). Functional Flt3 domains were identified based on the alignment with human FLT3 (29). Three-dimensional homology models of the extracellular Flt3 domains and 4-helix cytokine–like cores of Flt3lg from *X. laevis* S and L homoeologs and *X. tropicalis* were compared using SWISS-MODEL protein modeling server (38).

Relative gene expression

RNA extraction, cDNA synthesis, and quantitative reverse transcription–PCR (RT-qPCR) analysis were realized as previously described (39). The expression level of each gene was normalized to *gapdh* endogenous control and then normalized against the lowest observed expression among all tested tissues including both S and L homoeologous genes. Homoeologous-specific primers were designed using Primer-BLAST (https://www.ncbi.nlm.nih.gov/tools/primer-blast/). Primer specificities were assessed by analyzing PCR products on 2% agarose gel and RT-qPCR melting curves. All primers used are listed in Supplemental Table I.

Recombinant protein production

Tagged recombinant proteins were produced by cloning *X. laevis* extracellular Flt3lg.S and Flt3lg.L into pMIB/V5 His A vector (Thermo Fisher Scientific). Coding sequences were amplified using *X. laevis* cDNA by PCR (all primers used are listed in Supplemental Table I). HindIII and XhoI domains were inserted before double digestion (New England Biolabs) and T4 DNA ligase to insert in the plasmid vector (New England Biolabs). Sf9 insect cells were transfected using Cellfectin II (Invitrogen) and 1 μg of plasmid containing xlFlt3lg.S, xlFlt3lg.L, or xlCsf1.S (40). Large-scale protein production was performed in Sf-900 II serum-free medium supplemented with 10 μg/ml gentamicin. rFlt3lg.L and rFlt3lg.S were purified by Ni-NTA-agarose chromatography (Qiagen) as previously described (40). The recombinant enriched fractions supplemented with 0.02% NaN_3 and cOmplete EDTA-free protease inhibitor cocktail (Roche) were stored at 4°C or −20°C for short- and long-term storage, respectively.

Cell isolation and flow cytometry

Splenocytes (200,000) harvested using a 70-μm nylon mesh were stained with 4 ng/μl enriched rFlt3lg.S or rFlt3lg.L or rCsf1.S in staining buffer for 1 h on ice as previously described (40, 41). Costaining was performed using *Xenopus*-specific biotinylated anti-CD8 (AM22), anti–MHC-II (AM20), and anti–IgM-Alexa Fluor 680 (10A9). Prior to flow cytometry measurement, stained cells were incubated with 15 pg of DAPI (BD Pharmingen) to stain and therefore exclude dead cells. Flow cytometry was performed on an LSR II flow cytometer (BD Biosciences). Analysis was carried on using the FCS Express 7 software (De Novo).

Western blot

Adult splenocytes (5×10^5) were incubated in amphibian phosphate saline buffer supplemented with 500 ng/ml rFlt3lg.S or rFlt3lg.L for 5, 15, 30 and 60 min at 27°C, then centrifuged for 1 min at 13,000 × *g* at 4°C. Cell pellets were lysed in 125 μl of immunoprecipitation lysis buffer (Thermo Scientific Pierce) supplemented with protease inhibitor mixture (cOmplete, Roche), phosphatase inhibitors II and III (Sigma-Aldrich), and 1% SDS. Cell debris was removed by centrifugation at 16,000 × *g* during 8 min at 4°C. After boiling the supernatant in 4× loading buffer with 2-ME for 10 min, the samples were loaded on 12% acrylamide gels for electrophoresis and then transferred onto polyvinylidene difluoride membranes. The membranes were blocked using EveryBlot blocking buffer (Bio-Rad) for 1 h at room temperature and probed overnight at 4°C with p-Erk1/2 (Thr^{202}/Tyr^{204}) Ab (Cell Signaling Technology, no. 9101) at 1:1000 dilution or Grp94 mAb

(Thermo Fisher Scientific, clone 9G10.F8.2) at 1:200 dilution in blocking buffer. The membranes were washed three times with TBS supplemented with 0.1% Tween 20 (TBST) and incubated for 1 h at room temperature with goat anti-rabbit or anti-rat IgG (H+L) Abs conjugated with HRP (Thermo Fisher Scientific) at 1:1000 dilution in blocking buffer. After three washes with TBST, the membranes were incubated for 5 min with Super-Signal West Femto maximum sensitivity substrate (Thermo Fisher Scientific) and imaged using a Bio-Rad ChemiDoc instrument. Chemiluminescent signals were analyzed by measuring the peak area using ImageJ (National Institutes of Health, 1.53k).

Statistical analysis

Expression levels of *flt3* and *flt3lg* homoeologs were analyzed using the Mann–Whitney *U* test. For gene expression, comparisons between the FACS-sorted cells the Kruskal–Wallis test followed by the multiple step-up method of Benjamini, Krieger, and Yekutieli were used. The results were considered significant at an α level of 5% ($p < 0.05$). All statistical analyses were carried out using GraphPad Prism 9 software (GraphPad Software).

Results

Evolutionary relationships of flt3/flt3lg *orthologs*

We first compared gene syntenies of *flt3* and *flt3lg* genomic regions in *X. laevis* with those of the related diploid *X. tropicalis*, as well as with *Homo sapiens*, *Callorhinchus milii*, *Latimeria chalumnae*, *Danio rerio*, and *Takifugu rubripes*. Although the gene synteny of *flt3* loci has been preserved among all the species considered, including both *X. laevis* homoeologs L and S (Fig. 1), *flt3lg* loci revealed signs of segment recombination events (Fig. 2). Importantly, Flt3lg genes have conserved proximity with *slc17a7*, *pih1d1*, and *aldh16a* among tetrapods and elasmobranch species, but not teleost fish (e.g., *Danio rerio*, *Takifugu rubripes, Oncorhynchus mykiss*, *Nothobranchius furzeri*, *Oreochromis niloticus*, and *Larimichthys crocea*; Fig. 2 and data not shown). The *flt3* high degree of conservation is also supported by phylogenetic analysis of deduced coding amino acid sequences, where the phylogenetic tree topology matching the species evolutionary history is robust (e.g., high bootstrap support; Supplemental Fig. 1). In contrast, Flt3lg phylogeny appears to be less robust and subjected to more diversity (Supplemental Fig. 1).

To gather additional insights into structural relationships among the different molecules, we conducted in silico conformation modeling. The Flt3 architecture including the extracellular domain with five Ig-like domains (D1–D5), the transmembrane, and the tyrosine kinase domains is conserved in *X. laevis* Flt3.S and Flt3.L (Fig. 3). All of the cysteines involved in the Ig folding via disulfide bonds in D1, D2, D3, and D4 are conserved among *X. laevis,* humans, and other jawed vertebrate species (29). However, cysteine residues are not

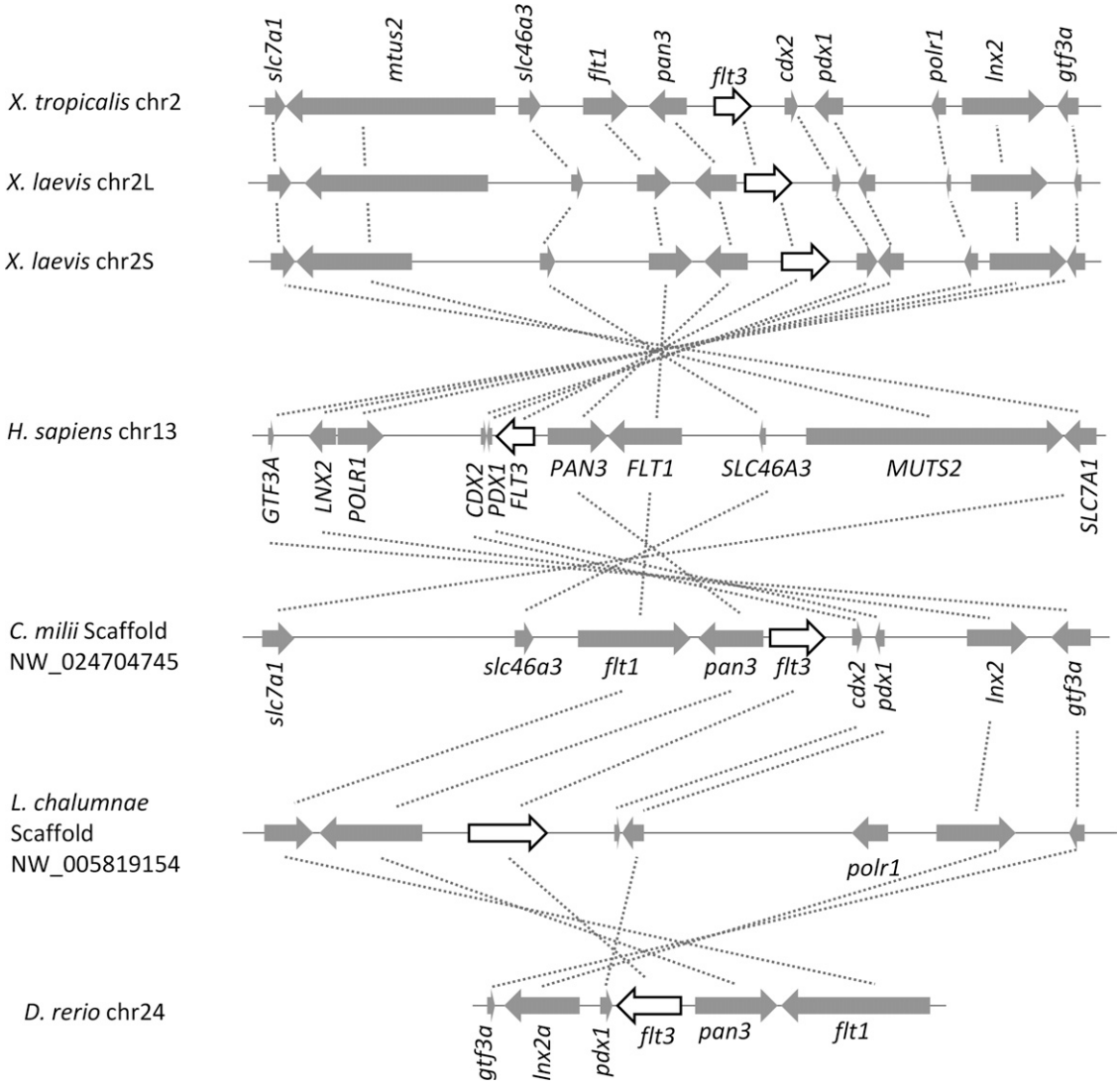

FIGURE 1. *Flt3* synteny analysis in jawed vertebrates. The *flt3* genomic locus in two amphibians (*X. laevis* and *X. tropicalis*), a mammal (*H. sapiens*), a cartilaginous fish (*C. milii*), and a lobed and ray-finned fish (*L. chalumnae* and *D. rerio*) are shown. Data were compiled using genome viewer pages on NCBI, Ensembl, and Xenbase.

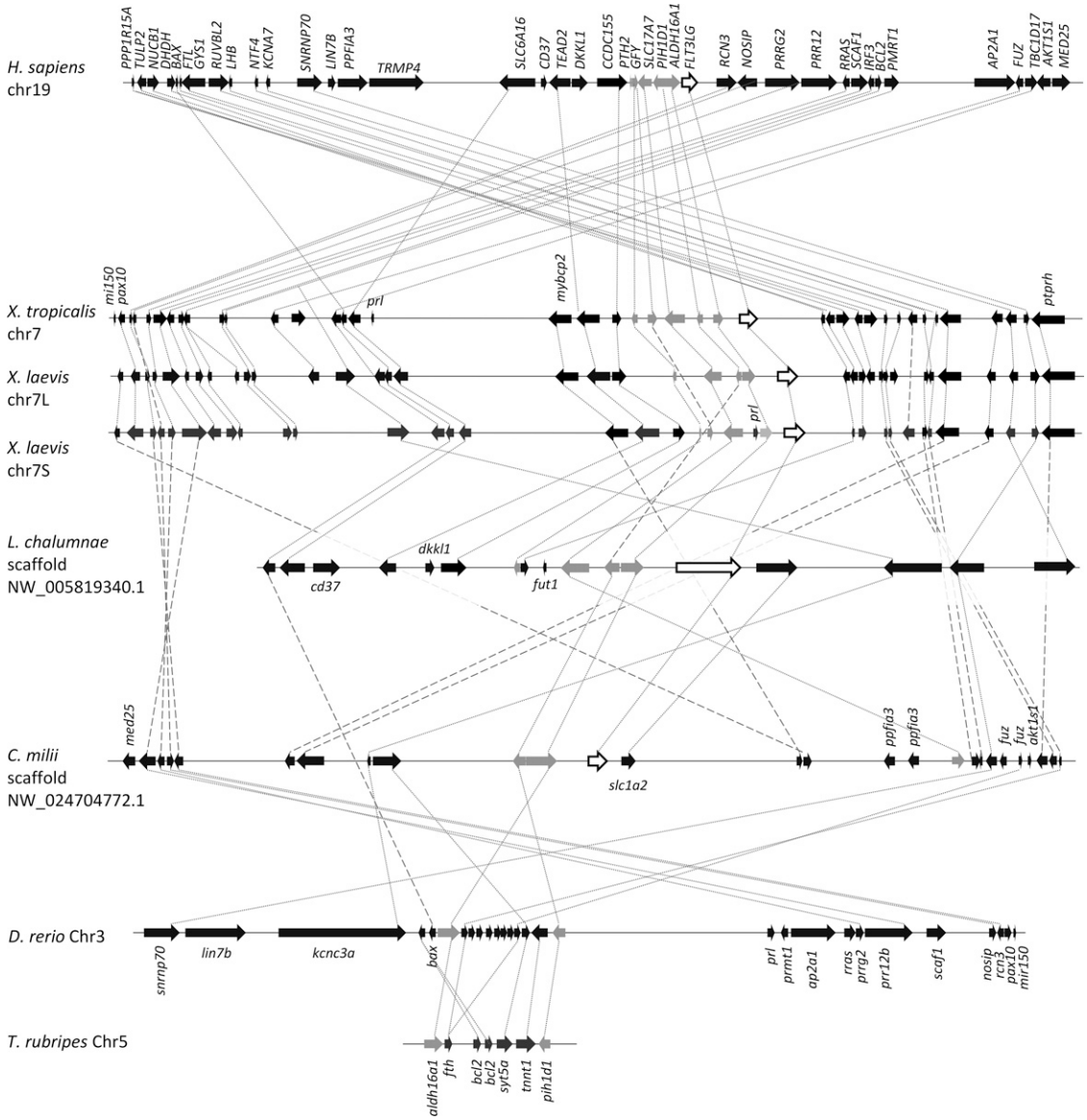

FIGURE 2. *Flt3lg* synteny analysis in jawed vertebrates. Flt3lg gene locus in two amphibians (*X. laevis* and *X. tropicalis*), a mammal (*H. sapiens*), a cartilaginous fish (*C. milii*), and a lobed and ray-finned fish (*L. chalumnae* and *D. rerio*) are shown. The Flt3lg gene is flanked in 3′ by *slc17a7*, *pih1d1*, and *aldh16a* in all Gnathostomata except for ray-finned fish. Data were compiled using genome viewer pages on NCBI, Ensembl, and Xenbase.

conserved on the D2 in different amphibian species, including *X. tropicalis*, and in fish. Additionally, D1 and D2 have been lost in two cartilaginous fish (*Carcharodon carcharias* and *C. milii*; Fig. 3A). Differently from the other RTKIII/V humans, the combined D1–D4 domains form an open horseshoe ring with D2 leaning against D3. D2 and D3 interaction is mediated by hydrophobic amino acids, which are evolutionarily conserved in jawed vertebrates whose D1 and D2 domains are conserved (Fig. 3A). Additionally, the amino acids involved in D3 and D4 hydrophobic interaction, as well as the linker residues that form an elbow, are conserved. This elbow domain is conserved among all RTKIII/Vs and is likely important for homotypic receptor conformation. Whereas in humans, FLT3LG binds to D3 of FLT3, it is divergent in the *Xenopus* model and in other jawed vertebrates. As highlighted in Fig. 3, a single residue of Flt3 at the interface with Flt3lg is conserved. Interestingly, lobed and ray-fined fish appear to have lost this evolutionarily conserved hydrophobic residue (F281 in humans) forming the ligand-binding epitope in humans.

Pairwise structure superpositions of the extracellular domains of the two *X. laevis* and the single *X. tropicalis* Flt3 suggest that D3, which represents the putative Flt3lg binding domain, is more divergent in Flt3.L than Flt3.S and *X. tropicalis* (xt)Flt3 (Fig. 3C). Interestingly, amino acid sequences of the extracellular Flt3.S and Flt3.L domains show a higher percentage of identity between *X. laevis* homoeologs than with the Flt3 of *X. tropicalis* (Table I). *Xenopus* extracellular Flt3 shows relatively low percentage of identities (~35%) with the human and mouse counterparts.

Based on in silico analysis, the *Xenopus* Flt3lg molecules are composed of a four-helix bundle or short chain helical cytokine fold, a transmembrane, and an intracellular domain as in humans. Examination of amino acid residues, which are critical for the bioactivity, structure, and dimerization of the human FLT3LG, indicates that these residues are largely conserved in *X. tropicalis* and the two *X. laevis* homoeologs (Fig. 4A) (29, 42, 43). However, the Flt3 binding domain, which is well conserved across tetrapods, has become more divergent for the L homeolog with the insertion of 3 aa (Fig. 4A) (29). Furthermore, analysis by structure superposition of the “hot spot” identified in humans by

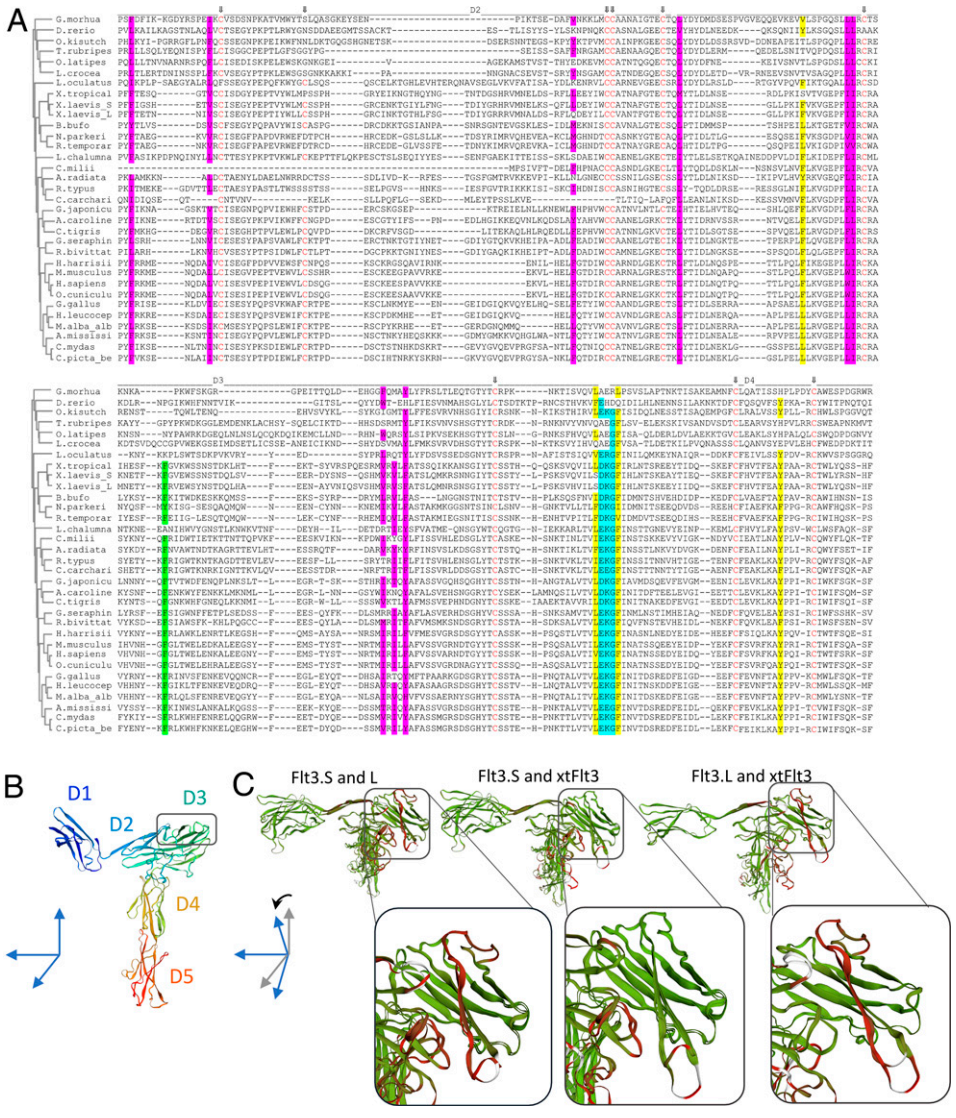

FIGURE 3. Predicted extracellular Flt3 architecture in jawed vertebrate based on the human Flt3 crystal structure. (**A**) Multiple amino acid alignment of the predicted partial extracellular Flt3 (D2–D4) from various jawed vertebrates including amphibians, mammals, reptiles, birds, and cartilaginous, ray-finned, and lobed finned fish. (⇩) Conserved cysteine residues are in red letters. Residues highlighted in green are at the interface with FLT3LG. Residues highlighted in purple are involved in the hydrophobic interaction between D2 and D3. Residues highlighted in yellow mediate hydrophobic interaction between D3 and D4. The residues highlighted in blue represent linker residues between D3 and D4 (29). (**B**) Folding model of the five Ig-like Flt3 extracellular domains D1–D5. The black box highlights the Flt3lg-binding epitope identified in humans. (**C**) Deduced pairwise structure superpositions of the Flt3.S, Flt3.L, and Flt3 of *X. tropicalis* (xtFlt3) emphasizing the putative Flt3lg-binding epitopes. Red and white of the cartoon alignment indicate local deviation in the protein structures and presence of extra amino acids, respectively.

amino acid substitution and in vitro bioactivity reveals that the structure of these domains is markedly divergent between Flt3lg.S and Flt3lg.L (Fig. 4). Interestingly, amino acid sequences of Flt3lg four-helix cytokine-like cores show a higher percentage of identity between the *X. laevis* homoeologs than with Flt3lg of *X. tropicalis* (Table I). *Xenopus* Flt3lg shows a relatively low percentage of identity (~30%) with the human and mouse counterparts (Table I).

Differential expression of X. laevis flt3/flt3lg *homoeologs*

To obtain evidence of distinctive functions of the two pairs of *flt3/flt3lg* homoeologs, we determined their relative gene expression patterns in various organs of tadpoles and adult frogs (Fig. 5). In tadpoles, the relative *flt3*.L expression in spleen was significantly more elevated than *flt3*.S (p = 0.0022). In adult spleen as well as in liver, *flt3*.L transcript levels were significantly higher than those of *flt3*.S (p = 0.0079) and tended to be more abundant in the bone marrow (p = 0.2856). It is also noteworthy that the increased transcript levels of *flt3*.L over the *flt3*.S homeolog were 130-fold higher in tadpole spleen versus only 10-fold in adults. Further differential expression between *flt3*.L over *flt3*.S homoeologs was detected in kidney and in thymus of adults (p = 0.0152 and p = 0.0411, respectively). Inversely, *flt3*.S was more expressed than *flt3*.L in the brain and thymus of tadpoles (p = 0.0022 and p = 0.0411, respectively).

For Flt3lg gene homoeologs, *flt3lg*.L was significantly more expressed than *flt3lg*.S in the spleen of tadpoles (Fig. 5, p = 0.0022). Similarly, in adult spleen as well as in the bone marrow, *flt3lg*.L was significantly more expressed than *flt3lg*.S (p = 0.0159 and p = 0.0079, respectively). Also, *flt3lg*.L transcript levels were significantly higher than those of *flt3lg*.S in tadpole adipose tissues (p = 0.0159), whereas no statistical difference in relative expression was detected between the two genes in adult skin and lung (p = 0.1143 and p = 0.0952). In

Table I. Percentage of amino acid sequence identity between Flt3 extracellular domains and Flt3lg predicted four-helix cytokine-like cores in *Xenopus*, mice, and humans

	*X. laevis*_S	*X. laevis*_L	*X. tropicalis*	*H. sapiens*	*M. musculus*
Flt3					
*X. laevis*_S					
*X. laevis*_L	81.8				
X. tropicalis	77.7	74.4			
H. sapiens	35.1	33.9	34.3		
M. musculus	36	34.3	35.1	84.3	
Flt3lg					
*X. laevis*_S					
*X. laevis*_L	71.3				
X. tropicalis	69.8	64.7			
H. sapiens	32.6	29.4	27.7		
M. musculus	28.7	25	29	73.9	

tadpoles, *flt3lg*.S was more expressed than *flt3lg*.L in liver and gills ($p = 0.0043$ and $p = 0.0031$).

Collectively, the differences in three-dimensional structure models among homeolog proteins and the changes in their developmental and tissue expression converge in suggesting a selective retention of this duplicated set for potential distinctive function.

Cellular characterization of X. laevis flt3 *homoeologs*

To investigate the cellular expression of the two *X. laevis* Flt3 homoeologs, we generated and produced tagged recombinant *X. laevis* Flt3lg.S and Flt3lg.L (rFlt3lg.S and rFlt3lg.L) in an insect expression system. Whereas partially purified rFlt3lg.L migrated as a unique band with an apparent molecular mass of 35 kDa on SDS-PAGE electrophoresis, rFlt3lg.S exhibited multiple bands of ~35 kDa, suggesting differences in posttranslational modifications (Fig. 6A). Based on the typical strong binding affinity of these ligands to their respective receptors, we used the tagged recombinant molecules to characterize cells expressing Flt3 at the cell surface (Flt3$^+$ cells) by flow cytometry and, after cell sorting, by RT-qPCR.

Flow cytometry analysis on *X. laevis* adult splenocytes with rFlt3lg.S and rFlt3lg.L, revealed that similar cell populations with comparable staining intensity were stained by each ligand (16.92 ± 9.33% for rFlt3lg.S versus 17.83 ± 10.24 for rFlt3lg.L$^+$; Fig. 6B). In comparison, the tagged recombinant Csf1r.S ligand *Xl*rCsf1.S produced in the same insect expression system stained only a minor fraction of the splenocytes from the same frogs (3.68 ± 1.39%; Fig. 6F, Supplemental Fig. 2). To substantiate these results, Flt3$^+$ cells costained with the *X. laevis*–specific anti-CD8 mAb were sorted for RT-qPCR analysis (Fig. 6C). Confirming the specificity of the staining, sorted rFlt3lg.S$^+$ and rFlt3lg.L$^+$ cells were markedly enriched in cells expressing high levels of *flt3*.S and *flt3*.L transcripts (Fig. 6D). It is noteworthy that significantly higher *flt3*.L transcript levels than for *flt3*.S were detected in the different splenic cell populations (Supplemental Fig. 3A). The binding of rFlt3lg.S and rFlt3lg.L to Flt3 was further validated by the rapid and transient phosphorylation of Erk1/2 triggered by the incubation of *X. laevis* splenocytes with rFlt3lg.S and rFlt3lg.L (Fig. 7).

Sorted rFlt3lg$^+$/CD8$^+$ splenocytes were found to express high levels of DC-SCRIPT transcript (*znf366*.L), as well as *xcr1.L*, *spi1.S/L*, *cxcl13*.S/L, and *ccl19*.S transcripts (Fig. 6D). These gene products are hallmarks of DC-like cells in *Xenopus* and chickens, as well as cDCs and FDCs in mammals (10, 18, 44–46). Furthermore, sorted rFlt3lg$^+$ cells expressed low transcript levels of the T cell marker *cd3g*.S (Supplemental Fig. 3B). Multiparametric flow cytometry analysis using different *X. laevis*–specific mAbs with rFlt3lg ligands identified a cell subset corresponding to a recently described dual FDC/DC subset named XL cells in *X. laevis* (10). This subset was characterized MHC-II^{bright} (Fig. 6E) with a higher size and complexity (i.e., forward scatter and side scatter) as reported for XL cells (Supplemental Fig. 2). This cell subset was also positively stained by anti-IgM and IgY mAbs as previously reported for XL cells (Fig. 6F, Supplemental Fig. 2). CD8 costaining further indicated that this putative XL cell

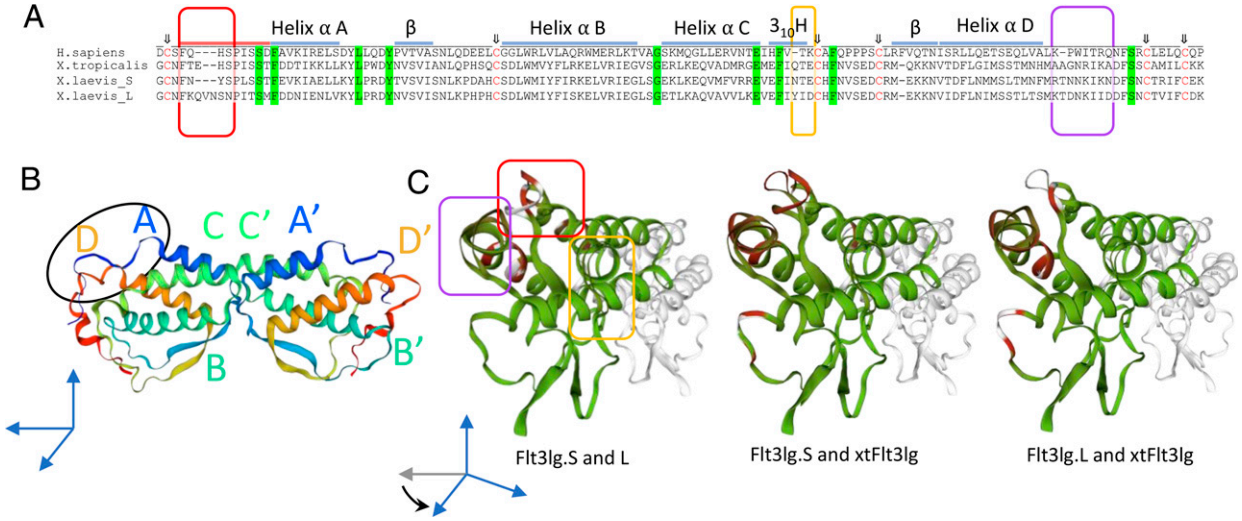

FIGURE 4. Predicted architecture of the four-helix cytokine-like cores of *Xenopus* Flt3lgs based on the crystal structure of human orthologs (29). (**A**) Multiple alignment of the deduced primary structures of Flt3lg.S, Flt3lg.L, and *X. tropicalis* (xt)Flt3lg with the human FLT3LG. (⇩) Conserved cysteine residues are in red letters. A red line above the sequences indicates residues in the conserved N-terminal receptor-binding loop. A blue line above the sequences indicates residues forming secondary structures as indicated. The residues highlighted in green are conserved residues important for human FLT3LG bioactivity (42, 43). Red, yellow, and violet empty boxes indicate segments that, in humans, highly influence binding and biological activity. (**B**) Cartoons of *Xenopus* Flt3lg predicted tertiary and quaternary structures. The black circle shows the close localization of the three segments highlighted in red, yellow, and violet in (A). (**C**) Deduced pairwise structure superpositions of the predicted *Xenopus* Flt3lg emphasizing the three domains important for Flt3lg binding and activity as highlighted in (A).

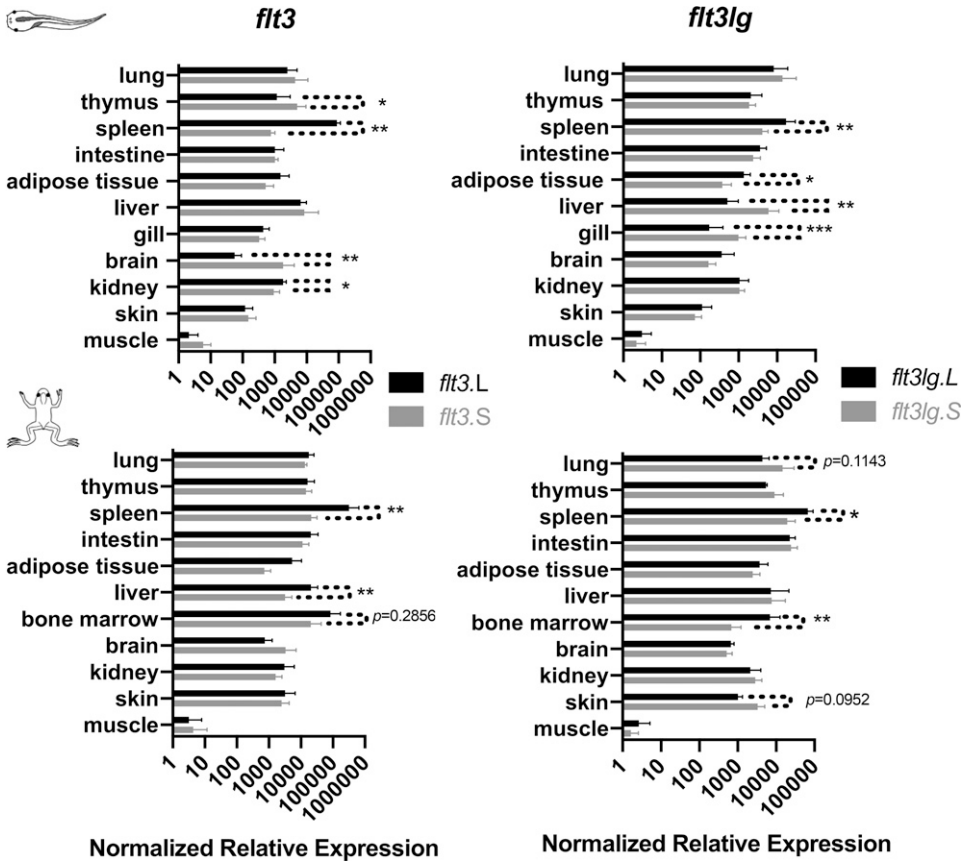

FIGURE 5. Tissue expression profiles of *flt3* and *flt3lg* homoeologs in *X. laevis* tadpoles and adult frogs. Normalized relative gene expression was determined by RT-qPCR as fold increase relative to *gapdh* endogenous control and normalized to the maximum ΔCt among all tested tissues including homoeologous pairs. Bars represent means and SD; $n = 5–6$ animals. Statistical differences between homoeologs were assessed using a Mann–Whitney *U* test: $*p < 0.05$, $**p < 0.001$.

population was $CD8^+$ but at a lower level than CD8 T cells (Fig. 6F, Supplemental Fig. 2). RT-qPCR analysis did not reveal significant differences of *cd8a*.L or *cd8b*.L transcript levels between $rFlt3lg^+CD8^+$ and $rFlt3lg^+$ sorted cells (Supplemental Fig. 3B). To further characterize these putative XL cells and distinguish them from macrophages, splenocytes were costained with rCsf1.S, which stains $Csf1r.S^+$ macrophages (39). We detected a subpopulation (0.65 ± 0.27% SD) of total splenocytes that was $Csf1r.S^+$, $MHC\text{-}II^+$ intermediate and $CD8^{dim}$. Finally, Flt3 ligands also stained a fraction of B cells as shown by high *ighm*.L transcripts levels in sorted rFlt3lg.S and $rFlt3lg.L^+$ cells, as well as cell surface-positive IgM costaining (Fig. 6D, 6E). The frequency of IgM^+ B cells costained with rFlt3lg.S and rFlt3lg.L varied considerably among the frogs tested (59.04 ± 18.85% and 57.30 ± 20.38%, respectively).

Discussion

In the present study, we were able to extend the identification of *flt3lg* orthologs in conserved syntenic genomic regions to cartilaginous fish and lobed finned fish (Sarcopterygii), but not ray-finned fish (Actinopterygii). This suggests that this gene and the genomic locus have undergone substantial alteration during fish evolution. The multiple inversions, a sign of recombination events, observed in the *flt3lg* syntenic regions as well as the amino acid sequence divergences across the different taxa examined are consistent with this idea (47). Additionally, we observed that the putative binding domain of Flt3lg on Flt3 considerably diverged across vertebrates, especially in lobed and ray-finned fish. The additional whole-genome duplication that occurred during the emergence of ray-finned fish 350 MYA probably increased the evolution rate of the Flt3lg gene and the genomic locus (recombination and mutation), preventing the identification of any putative Flt3lg-like gene homologs in these taxa using current BLAST- and synteny-based searches.

In contrast to teleost fish, two sets of Flt3/Flt3lg genes have been retained in *X. laevis* subsequently to the whole-genome duplication that occurred 17–18 MYA. The corresponding syntenic regions of L and S chromosomes of *X. laevis*, and of *X. tropicalis*, are conserved with humans. Comparison of the deduced primary structures indicates that *X. laevis* gene homoeologs are more closely related than with the respective *X. tropicalis* homologs. This is consistent with the fact that the speciation divergence of *X. laevis* and *X. tropicalis* is estimated to have occurred 48 MYA, whereas the speciation resulting in L and S progenitors is estimated to date back 34 MYA (33). The latter event was followed by a hybridization step resulting in *X. laevis* allotetraploidization 17–18 MYA (33). Because of their more recent emergence, the primary structures of the S and L homoeologs are more closely related than with the primary structure of *X. tropicalis*. However, analysis of the predicted tertiary structures suggests that the conformation of proteins encoded by genes on the S chromosome are more related to the *X. tropicalis* orthologs, which would imply that allotetraploidization has allowed *flt3*.L and *flt3lg*.L to diverge, coevolve, and subfunctionalize from their S counterpart. In this regard, only the Flt3lg.S homeolog shows a different degree of posttranslational modification, which is likely important for protein conformation and function. In comparison, the recombinant human Flt3lg shows signs of *N*- and *O*-glycosylation (48). Considering the Flt3/Flt3lg cell signaling pathway, the apparent higher capacity of Flt3lg.S to trigger p-Erk1/2 might be due to different expression levels in the insect expression system or different purities. From tadpoles to frogs, the major site for hematopoiesis is located in the subcapsular region of the liver where erythropoiesis

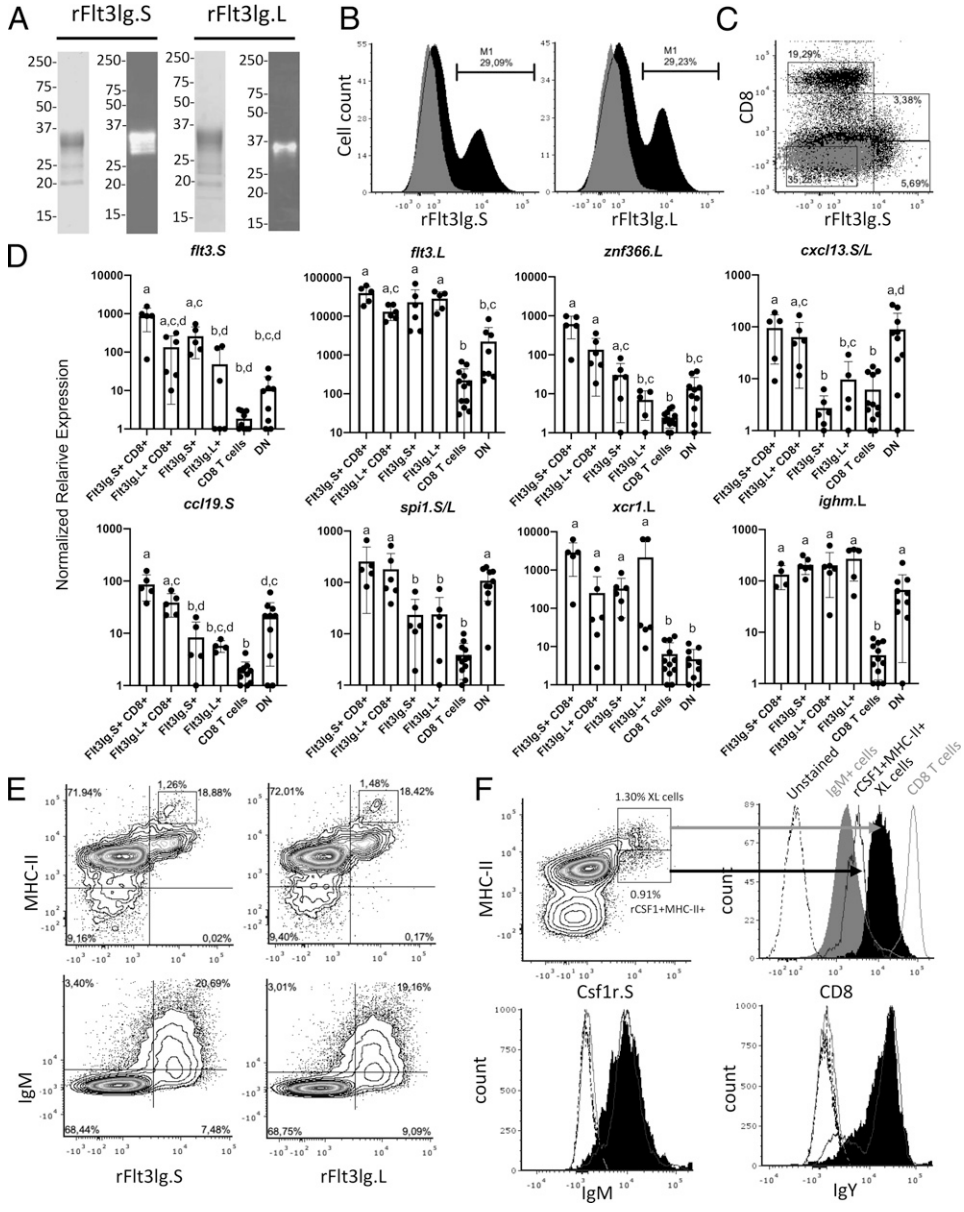

FIGURE 6. Characterization of rFlt3lg.S$^+$ and rFlt3lg.L$^+$ cells by flow cytometry and RT-qPCR. (**A**) Coomassie staining and associated Western blot of purified rFlt3lg.S and rFlt3lg.L after SDS-PAGE. (**B**) Histograms (black peak) of rFlt3lg.S- or rFlt3lg.L-stained adult splenocytes. Gray indicates isotype controls. (**C**) Flow cytogram showing the gating strategy used to sort the different populations analyzed by RT-qPCR. Splenocytes were costained with either rFlt3lg.S or rFlt3lg.L and anti-CD8 mAb to sort double-positive rFlt3lg.S$^+$ or rFlt3lg.L$^+$/CD8$^+$, single-positive rFlt3lg.S$^+$, rFlt3lg.L$^+$, and CD8$^+$ T cells. (**D**) RT-qPCR analysis of the Flt3.S and Flt3.L genes as well as gene markers for *Xenopus* DC-like XL cells (*ccl19*.S, *spi1*.S/L, and *cxcl13*.S/L), mammalian cDCs (*ccl19*.S, *spi1*.S/L, *znf366*.L, and *xcr1*.L), FDCs (*cxcl13*.S/L), and B cells (*ighm*.L). Normalized relative gene expression was determined as fold increase relative to *gapdh* endogenous control and normalized to the maximum ΔCt among samples from all sorted populations. Bars represent means and SD. Letters (a–c) indicate statistically significant differences among experimental groups ($n = 6$, two independent experiments, $p < 0.05$) using a nonparametric Kruskal–Wallis test followed by the multiple step-up method of Benjamini, Krieger, and Yekutieli). (**E**) Flow cytograms of rFlt3lg.S$^+$, rFlt3lg.L$^+$, MHC-II, and IgM *X. laevis* mAbs costaining. (**F**) Flow cytograms of Csf1r$^+$ MHC-II$^+$ cells and Csf1r$^+$ MHC^{high} XL cells costained with IgM and IgY *X. laevis* mAbs. CD8, IgY, and IgM staining histograms of Csf1r$^+$ MHC^{high} XL cells (filled area in black), Csf1r$^+$ MHC-II$^+$ cells (black with empty area), IgM$^+$ cells (filled area in gray), CD8 T cells (gray with empty area) and isotype control (black dotted line) are shown.

also takes place (49). In contrast to mammals, the *X. laevis* bone marrow, which develops after metamorphosis, appears to mainly harbor the final steps of myelopoiesis (40, 50). Considering lymphopoiesis, although the role of thymus in T cell development is well known, the site of common lymphoid progenitors and B cell lymphopoiesis remained to be fully investigated in adults and tadpoles (51, 52). Although histological studies in adults have shown that bone marrow hematopoietic cells are mostly represented by myeloid progenitors, low levels of *rag1* and *rag2* transcripts have been detected (53–55). In tadpoles, B cells have been suggested to have developed in the liver (51). Gene expression analysis revealed that in adult frogs *flt3lg*.L is significantly more expressed by nonstromal bone marrow cells than its counterpart from the S chromosome, whereas *flt3*.L is more expressed than the S homoeologs in the liver of adults. In contrast, in tadpoles *flt3lg*.S is more expressed than the L homeolog in the liver. We interpret these data as evidence of subfunctionalization where Flt3/Flt3lg.L gene homoeologs may play a more important role in adult hematopoiesis, whereas Flt3/Flt3lg.S gene homoeologs may have a preponderant role in the larval hematopoiesis. Additionally, the

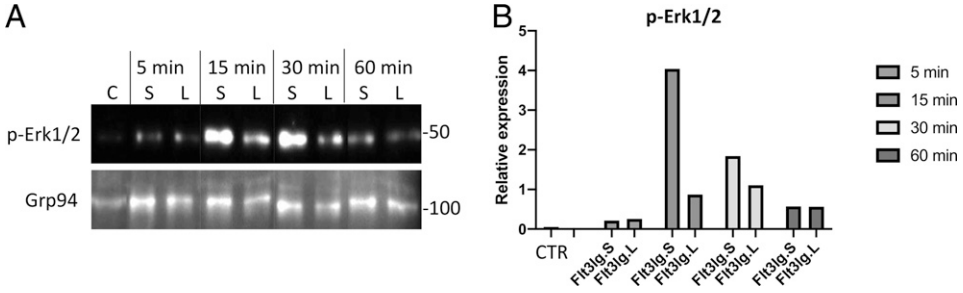

FIGURE 7. Western blot analysis of the Flt3/Flt3lg-mediated cell signal transduction. (**A**) p-Erk1/2 and Grp94 detection on *X. laevis* splenocytes after 5, 15, 30, and 60 min of incubation with rFlt3lg.S or rFlt3lg.L at 27°C. (**B**) Relative p-Erk1/2 expression to Grp94 quantified using ImageJ.

higher expression of Flt3/Flt3lg.L gene homoeologs in the tadpole and adult spleens as well as in adult splenocytes suggest a preponderant role in immune cell homeostasis. Interestingly, Flt3 and its ligand Flt3lg are also involved in mammalian neuron function and may play a role in the development of the nervous system (56, 57). Although Flt3 and Flt3lg genes are also expressed in the brain of *X. laevis*, the higher *flt3*.S transcript levels compared with the L counterpart in the brain of *X. laevis* tadpoles could imply a preferential role of this L homeolog during neural development in *X. laevis*. Although the distinctive differential expression of the two sets of Flt3/Flt3lg genes is consistent with a subfunctionalization, it is noteworthy that in vitro, rFlt3lg.S and rFlt3lg.L bind to both Flt3.S and Flt3.L, which implies that these homeolog genes still perform a partial overlapping function.

Outside of mammals, little is still known about Flt3lg/Flt3 function, particularly regarding DC biology. To fill this knowledge gap, we used *X. laevis* recombinant tagged Flt3lgs as reagents to identify and characterize immune cell population expressing Flt3 at their surface. Notably, we found that XL cells were brightly stained with rFlt3lg.S and rFlt3lg.L, indicating high levels of Flt3 surface expression by these cells, which is reminiscent of the mammalian cDCs and chicken DCs (19, 58). In addition to the high expression of surface MHC-II, expression of Flt3 on XL cells was confirmed by the enrichment with the Flt3lg staining of cells highly expressing XL cell markers, that is, mammalian FDC marker (*cxcl13*) or cDC markers (*spi1*, *ccl19*). The additional detection of surface Csf1r.S expression by these cells reinforces previous work suggesting the dual hematopoietic and myeloid lineage of XL cells (10). It is noteworthy that mice and chicken cDCs are also Csf1r$^+$ (19, 59). The staining of XL cells with anti-IgM is likely due to *X. laevis* IgM bound to Fcamr, which is expressed at the XL cell surface, although the Fcr responsible for the IgY binding has not been identified to date (60). Our gene expression analysis suggests that XL cells express high levels of DC-SCRIPT (*znf366*.L) as in human cDC1s, mouse cDC1s, and fish DC-like cells (17, 61–63), as well as *xcr1.L* also produced by human and mouse cDC1s and chicken DC-like cells (18, 19, 64). Finally, our flow cytometry analysis shows that XL cells are CD8$^+$ similar to cDC1s in mice (64). Based on these data we propose that XL cells and jawed vertebrate DCs are evolutionarily related and that ancient tetrapod DCs share common features of FDCs and cDCs.

Finally, the high expression of *ighm*.L transcript by Flt3$^+$ and Flt3$^-$ splenocytes suggests that Flt3 is expressed by a subpopulation of IgM$^+$ B cells in *X. laevis* as in mammals (65). In addition to its role in pro–B cell differentiation, Flt3 is a marker of B cell activation and proliferation (65–67). More specifically, Flt3 has been found to be required for B cell maturation including class-switch recombination to IgG (65). Nevertheless, the role of Flt3 in B cell activation and differentiation remains to be fully characterized.

Acknowledgments

We thank Tina Martin for the expert animal husbandry and Ruth Serra-Moreno for precious advice on the Western blot experiment.

Disclosures

The authors have no financial conflicts of interest.

References

1. Chen, L., and D. B. Flies. 2013. Molecular mechanisms of T cell co-stimulation and co-inhibition. [Published erratum appears in 2013 *Nat. Rev. Immunol.* 13: 542.] *Nat. Rev. Immunol.* 13: 227–242.
2. Hogquist, K. A., and S. C. Jameson. 2014. The self-obsession of T cells: how TCR signaling thresholds affect fate "decisions" and effector function. *Nat. Immunol.* 15: 815–823.
3. Liu, J., X. Zhang, Y. Cheng, and X. Cao. 2021. Dendritic cell migration in inflammation and immunity. *Cell. Mol. Immunol.* 18: 2461–2471.
4. Flajnik, M. F. 2018. A cold-blooded view of adaptive immunity. *Nat. Rev. Immunol.* 18: 438–453.
5. Barreda, D. R., H. R. Neely, and M. F. Flajnik. 2017. Evolution of myeloid cells. In *Myeloid Cells in Health and Disease: A Synthesis.* S. Gordon, ed. American Society for Microbiology, Washington, DC, p. 43–58.
6. Soleto, I., U. Fischer, C. Tafalla, and A. G. Granja. 2018. Identification of a potential common ancestor for mammalian cross-presenting dendritic cells in teleost respiratory surfaces. *Front. Immunol.* 9: 59.
7. Lugo-Villarino, G., K. M. Balla, D. L. Stachura, K. Bañuelos, M. B. F. Werneck, and D. Traver. 2010. Identification of dendritic antigen-presenting cells in the zebrafish. *Proc. Natl. Acad. Sci. USA* 107: 15850–15855.
8. Vu Manh, T.-P., H. Marty, P. Sibille, Y. Le Vern, B. Kaspers, M. Dalod, I. Schwartz-Cornil, and P. Quéré. 2014. Existence of conventional dendritic cells in *Gallus gallus* revealed by comparative gene expression profiling. *J. Immunol.* 192: 4510–4517.
9. Baldwin III, W. M., and N. Cohen. 1981. A giant cell with dendritic cell properties in spleens of the anuran amphibian *Xenopus laevis*. *Dev. Comp. Immunol.* 5: 461–473.
10. Neely, H. R., J. Guo, E. M. Flowers, M. F. Criscitiello, and M. F. Flajnik. 2018. "Double-duty" conventional dendritic cells in the amphibian *Xenopus* as the prototype for antigen presentation to B cells. *Eur. J. Immunol.* 48: 430–440.
11. Kazi, J. U., and L. Rönnstrand. 2019. FMS-like tyrosine kinase 3/FLT3: from basic science to clinical implications. *Physiol. Rev.* 99: 1433–1466.
12. Verstraete, K., and S. N. Savvides. 2012. Extracellular assembly and activation principles of oncogenic class III receptor tyrosine kinases. *Nat. Rev. Cancer* 12: 753–766.
13. Grafone, T., M. Palmisano, C. Nicci, and S. Storti. 2012. An overview on the role of FLT3-tyrosine kinase receptor in acute myeloid leukemia: biology and treatment. *Oncol. Rev.* 6: e8.
14. Tsapogas, P., C. J. Mooney, G. Brown, and A. Rolink. 2017. The cytokine Flt3-ligand in normal and malignant hematopoiesis. *Int. J. Mol. Sci.* 18: 1115.
15. Brunet, F. G., J.-N. Volff, and M. Schartl. 2016. Whole genome duplications shaped the receptor tyrosine kinase repertoire of jawed vertebrates. *Genome Biol. Evol.* 8: 1600–1613.
16. He, B.-L., X. Shi, C. H. Man, A. C. H. Ma, S. C. Ekker, H. C. H. Chow, C. W. E. So, W. W. L. Choi, W. Zhang, Y. Zhang, and A. Y. H. Leung. 2014. Functions of flt3 in zebrafish hematopoiesis and its relevance to human acute myeloid leukemia. *Blood* 123: 2518–2529.
17. Guslund, N. C., M. H. Solbakken, M. S. O. Brieuc, S. Jentoft, K. S. Jakobsen, and S.-W. Qiao. 2020. Single-cell transcriptome profiling of immune cell repertoire of the Atlantic cod which naturally lacks the major histocompatibility class II system. *Front. Immunol.* 11: 559555.
18. Sutton, K. M., K. M. Morris, D. Borowska, H. Sang, P. Kaiser, A. Balic, and L. Vervelde. 2021. Characterization of conventional dendritic cells and macrophages in the spleen using the CSF1R-reporter transgenic chickens. *Front. Immunol.* 12: 636436.
19. Wu, Z., T. Hu, C. Chintoan-Uta, J. Macdonald, M. P. Stevens, H. Sang, D. A. Hume, P. Kaiser, and A. Balic. 2022. Development of novel reagents to chicken FLT3,

XCR1 and CSF2R for the identification and characterisation of avian conventional dendritic cells. *Immunology* 165: 171–194.
20. Karsunky, H., M. Merad, A. Cozzio, I. L. Weissman, and M. G. Manz. 2003. Flt3 ligand regulates dendritic cell development from Flt3$^+$ lymphoid and myeloid-committed progenitors to Flt3$^+$ dendritic cells in vivo. *J. Exp. Med.* 198: 305–313.
21. Manfra, D. J., S.-C. Chen, K. K. Jensen, J. S. Fine, M. T. Wiekowski, and S. A. Lira. 2003. Conditional expression of murine Flt3 ligand leads to expansion of multiple dendritic cell subsets in peripheral blood and tissues of transgenic mice. *J. Immunol.* 170: 2843–2852.
22. Maraskovsky, E., K. Brasel, M. Teepe, E. R. Roux, S. D. Lyman, K. Shortman, and H. J. McKenna. 1996. Dramatic increase in the numbers of functionally mature dendritic cells in Flt3 ligand-treated mice: multiple dendritic cell subpopulations identified. *J. Exp. Med.* 184: 1953–1962.
23. McKenna, H. J., K. L. Stocking, R. E. Miller, K. Brasel, T. D. Smedt, E. Maraskovsky, C. R. Maliszewski, D. H. Lynch, J. Smith, B. Pulendran, et al. 2000. Mice lacking flt3 ligand have deficient hematopoiesis affecting hematopoietic progenitor cells, dendritic cells, and natural killer cells. *Blood* 95: 3489–3497.
24. Shurin, M. R., P. P. Pandharipande, T. D. Zorina, C. Haluszczak, V. M. Subbotin, O. Hunter, A. Brumfield, W. J. Storkus, E. Maraskovsky, and M. T. Lotze. 1997. FLT3 ligand induces the generation of functionally active dendritic cells in mice. *Cell. Immunol.* 179: 174–184.
25. Chklovskaia, E., W. Jansen, C. Nissen, S. D. Lyman, C. Rahner, L. Landmann, and A. Wodnar-Filipowicz. 1999. Mechanism of flt3 ligand expression in bone marrow failure: translocation from intracellular stores to the surface of T lymphocytes after chemotherapy-induced suppression of hematopoiesis. *Blood* 93: 2595–2604.
26. Kenins, L., J. W. Gill, R. L. Boyd, G. A. Holländer, and A. Wodnar-Filipowicz. 2008. Intrathymic expression of Flt3 ligand enhances thymic recovery after irradiation. *J. Exp. Med.* 205: 523–531.
27. Lisovsky, M., S. E. Braun, Y. Ge, H. Takahira, L. Lu, V. G. Savchenko, S. D. Lyman, and H. E. Broxmeyer. 1996. Flt3-ligand production by human bone marrow stromal cells. *Leukemia* 10: 1012–1018.
28. Miloud, T., N. Fiegler, J. Suffner, G. J. Hämmerling, and N. Garbi. 2012. Organ-specific cellular requirements for in vivo dendritic cell generation. *J. Immunol.* 188: 1125–1135.
29. Verstraete, K., G. Vandriessche, M. Januar, J. Elegheert, A. V. Shkumatov, A. Desfosses, K. Van Craenenbroeck, D. I. Svergun, I. Gutsche, B. Vergauwen, and S. N. Savvides. 2011. Structural insights into the extracellular assembly of the hematopoietic Flt3 signaling complex. *Blood* 118: 60–68.
30. Rivers-Auty, J., M. J. D. Daniels, I. Colliver, D. L. Robertson, and D. Brough. 2018. Redefining the ancestral origins of the interleukin-1 superfamily. *Nat. Commun.* 9: 1156.
31. Heeb, L. E. M., C. Egholm, and O. Boyman. 2020. Evolution and function of interleukin-4 receptor signaling in adaptive immunity and neutrophils. *Genes Immun.* 21: 143–149.
32. Soltis, P. S., and D. E. Soltis, eds. 2012. *Polyploidy and Genome Evolution*. Springer, Berlin.
33. Session, A. M., Y. Uno, T. Kwon, J. A. Chapman, A. Toyoda, S. Takahashi, A. Fukui, A. Hikosaka, A. Suzuki, M. Kondo, et al. 2016. Genome evolution in the allotetraploid frog *Xenopus laevis*. *Nature* 538: 336–343.
34. Saitou, N., and M. Nei. 1987. The neighbor-joining method: a new method for reconstructing phylogenetic trees. *Mol. Biol. Evol.* 4: 406–425.
35. Kumar, S., G. Stecher, M. Li, C. Knyaz, and K. Tamura. 2018. MEGA X: Molecular Evolutionary Genetics Analysis across computing platforms. *Mol. Biol. Evol.* 35: 1547–1549.
36. Stecher, G., K. Tamura, and S. Kumar. 2020. Molecular Evolutionary Genetics Analysis (MEGA) for macOS. *Mol. Biol. Evol.* 37: 1237–1239.
37. Corpet, F. 1988. Multiple sequence alignment with hierarchical clustering. *Nucleic Acids Res.* 16: 10881–10890.
38. Arnold, K., L. Bordoli, J. Kopp, and T. Schwede. 2006. The SWISS-MODEL workspace: a web-based environment for protein structure homology modelling. *Bioinformatics* 22: 195–201.
39. Samanta, M., J. Yim, F. De Jesús Andino, M. Paiola, and J. Robert. 2021. TLR5-mediated reactivation of quiescent ranavirus FV3 in *Xenopus* peritoneal macrophages. *J. Virol.* 95: e00215-21.
40. Grayfer, L., and J. Robert. 2013. Colony-stimulating factor-1-responsive macrophage precursors reside in the amphibian (*Xenopus laevis*) bone marrow rather than the hematopoietic subcapsular liver. *J. Innate Immun.* 5: 531–542.
41. Robert, J., E.-S. Edholm, and F. De Jesus Andino. 2018. Evaluating blood cell populations in Xenopus using flow cytometry and differential counts by cytospin. *Methods Mol. Biol.* 1865: 265–273.
42. Graddis, T. J., K. Brasel, D. Friend, S. Srinivasan, S. Wee, S. D. Lyman, C. J. March, and J. T. McGrew. 1998. Structure-function analysis of FLT3 ligand-FLT3 receptor interactions using a rapid functional screen. *J. Biol. Chem.* 273: 17626–17633.
43. Savvides, S. N., T. Boone, and P. Andrew Karplus. 2000. Flt3 ligand structure and unexpected commonalities of helical bundles and cystine knots. *Nat. Struct. Biol.* 7: 486–491.
44. Zhang, S., H. D. Coughlan, M. Ashayeripanah, S. Seizova, A. J. Kueh, D. V. Brown, W. Cao, N. Jacquelot, A. D'Amico, A. M. Lew, et al. 2021. Type 1 conventional dendritic cell fate and function are controlled by DC-SCRIPT. *Sci. Immunol.* 6: eabf4432.
45. Vu Manh, T.-P., J. Elhmouzi-Younes, C. Urien, S. Ruscanu, L. Jouneau, M. Bourge, M. Moroldo, G. Foucras, H. Salmon, H. Marty, et al. 2015. Defining mononuclear phagocyte subset homology across several distant warm-blooded vertebrates through comparative transcriptomics. [Published erratum appears in 2016 *Front. Immunol.* 7: 143.] *Front. Immunol.* 6: 299.
46. Crozat, K., R. Guiton, V. Contreras, V. Feuillet, C.-A. Dutertre, E. Ventre, T.-P. Vu Manh, T. Baranek, A. K. Storset, J. Marvel, et al. 2010. The XC chemokine receptor 1 is a conserved selective marker of mammalian cells homologous to mouse CD8α$^+$ dendritic cells. *J. Exp. Med.* 207: 1283–1292.
47. Pál, C., B. Papp, and M. J. Lercher. 2006. An integrated view of protein evolution. *Nat. Rev. Genet.* 7: 337–348.
48. Zhang, Y.-L., S.-S. Chen, K.-G. Yang, L. Su, Y.-C. Deng, and C.-Z. Liu. 2005. Functional expression, purification, and characterization of human Flt3 ligand in the *Pichia pastoris* system. *Protein Expr. Purif.* 42: 246–254.
49. Nogawa-Kosaka, N., T. Sugai, K. Nagasawa, Y. Tanizaki, M. Meguro, Y. Aizawa, S. Maekawa, M. Adachi, R. Kuroki, and T. Kato. 2011. Identification of erythroid progenitors induced by erythropoietic activity in *Xenopus laevis*. *J. Exp. Biol.* 214: 921–927.
50. Yaparla, A., E. S. Wendel, and L. Grayfer. 2016. The unique myelopoiesis strategy of the amphibian *Xenopus laevis*. *Dev. Comp. Immunol.* 63: 136–143.
51. Du Pasquier, L., J. Robert, M. Courtet, and R. Mussmann. 2000. B-cell development in the amphibian *Xenopus*. *Immunol. Rev.* 175: 201–213.
52. Robert, J., and Y. Ohta. 2009. Comparative and developmental study of the immune system in *Xenopus*. *Dev. Dyn.* 238: 1249–1270.
53. Greenhalgh, P., C. E. Olesen, and L. A. Steiner. 1993. Characterization and expression of recombination activating genes (RAG-1 and RAG-2) in Xenopus laevis. *J. Immunol.* 151: 3100–3110.
54. Morita, S., T. Moriishi, S. Matsunaga, K. Kitamura, S. I. Abe, and A. Yamaguchi. 2021. Characteristic distribution of hematopoietic cells in bone marrow of *Xenopus laevis*. *Bull. Tokyo Dent. Coll.* 62: 171–180.
55. Tanaka, Y. 1976. Architecture of the marrow vasculature in three amphibian species and its significance in hematopoietic development. *Am. J. Anat.* 145: 485–497.
56. Brazel, C. Y., M. H. Ducceschi, B. Pytowski, and S. W. Levison. 2001. The FLT3 tyrosine kinase receptor inhibits neural stem/progenitor cell proliferation and collaborates with NGF to promote neuronal survival. *Mol. Cell. Neurosci.* 18: 381–393.
57. Rivat, C., C. Sar, I. Mechaly, J.-P. Leyris, L. Diouloufet, C. Sonrier, Y. Philipson, O. Lucas, S. Mallié, A. Jouvenel, et al. 2018. Inhibition of neuronal FLT3 receptor tyrosine kinase alleviates peripheral neuropathic pain in mice. *Nat. Commun.* 9: 1042.
58. Cueto, F. J., and D. Sancho. 2021. The Flt3L/Flt3 axis in dendritic cell biology and cancer immunotherapy. *Cancers (Basel)* 13: 1525.
59. MacDonald, H. R., F. Radtke, and A. Wilson. 2001. T cell fate specification and αβ/γδ lineage commitment. *Curr. Opin. Immunol.* 13: 219–224.
60. Flowers, E. M., H. R. Neely, J. Guo, T. Almeida, Y. Ohta, C. D. Castro, and M. F. Flajnik. 2021. Identification of the Fc-alpha/mu receptor in *Xenopus* provides insight into the emergence of the poly-Ig receptor (pIgR) and mucosal Ig transport. *Eur. J. Immunol.* 51: 2590–2606.
61. Chopin, M., A. T. Lun, Y. Zhan, J. Schreuder, H. Coughlan, A. D'Amico, L. A. Mielke, F. F. Almeida, A. J. Kueh, R. A. Dickins, et al. 2019. Transcription factor PU.1 promotes conventional dendritic cell identity and function via induction of transcriptional regulator DC-SCRIPT. *Immunity* 50: 77–90.e5.
62. Triantis, V., V. Moulin, M. W. G. Looman, F. C. Hartgers, R. A. J. Janssen, and G. J. Adema. 2006. Molecular characterization of the murine homologue of the DC-derived protein DC-SCRIPT. *J. Leukoc. Biol.* 79: 1083–1091.
63. Zoccola, E., J. Delamare-Debouttéville, and A. C. Barnes. 2015. Identification of barramundi (*Lates calcarifer*) DC-SCRIPT, a specific molecular marker for dendritic cells in fish. *PLoS One* 10: e0132687.
64. Chrisikos, T. T., Y. Zhou, N. Slone, R. Babcock, S. S. Watowich, and H. S. Li. 2019. Molecular regulation of dendritic cell development and function in homeostasis, inflammation, and cancer. *Mol. Immunol.* 110: 24–39.
65. Svensson, M. N. D., K. M. E. Andersson, C. Wasén, M. C. Erlandsson, M. Nurkkala-Karlsson, I.-M. Jonsson, M. Brisslert, M. Bemark, and M. I. Bokarewa. 2015. Murine germinal center B cells require functional Fms-like tyrosine kinase 3 signaling for IgG1 class-switch recombination. *Proc. Natl. Acad. Sci. USA* 112: E6644–E6653.
66. Mackarehtschian, K., J. D. Hardin, K. A. Moore, S. Boast, S. P. Goff, and I. R. Lemischka. 1995. Targeted disruption of the flk2/flt3 gene leads to deficiencies in primitive hematopoietic progenitors. *Immunity* 3: 147–161.
67. Kallies, A., J. Hasbold, K. Fairfax, C. Pridans, D. Emslie, B. S. McKenzie, A. M. Lew, L. M. Corcoran, P. D. Hodgkin, D. M. Tarlinton, and S. L. Nutt. 2007. Initiation of plasma-cell differentiation is independent of the transcription factor Blimp-1. *Immunity* 26: 555–566.

Supplemental Table I. RT-qPCR and cloning primer sequences.

flt3lg.L cloning	Gene amplification	
	For: TGGGGCTCACTGCACAATTT	
	Rev: CCACTCTTGGCTCTATGCTGA	
	Plasmid insertion with HindIII and XhoI domains	
	For: GGGCTCGAAGCTTTCTCGTGCTTCTATTTCTGTT	
	Rev: GGGCTCGCTCGAGTGCTGATTCTTCTGTTCTTCTT	
	Extracellular domain selection	
	For: CACTCCAGACTCGAGTCTAGAGGGCCCT	
	Rev: TCTGGAGTGCTGCTCTTCCCCAATCTGTTTATTATC	
	For2: CTCGAGTCTAGAGGGCCCT	
	Rev2: CTGCTCTTCCCCAATCTGTTTATTATC	
flt3lg.S cloning	Gene amplification	
	For: CTGCATGATTTGGGGTACGTG	
	Rev: TTTGTCACTCTTGCCTCTCTGC	
	Plasmid insertion with HindIII and XhoI domains	
	For: GGGCTCGAAGCTTTCTCGTGCTTCTATTACTCTTG	
	Rev: GGGCTCGCTCGAGCTCTTGCCTCTCTGCTAAAT	
	Extracellular domain selection	
	For: CATAACTCCCTCGAGTCTAGAGGGCCCT	
	Rev: GGAGTTATGACCTTCCCCGGTCGG	
	For2: CTCGAGTCTAGAGGGCCCT	
	Rev2: ACCTTCCCCGGTCGG	
RT-qPCR	*fl3*.S For: CGTCCGACTTGGGGTGTTAC	Rev: TCTCTGAGCACCCAGCTACA
	flt3.L For: ATCATGTGTCTGGCTGCTCC	Rev: TATTCCCCGGCGTGTTTCTC
	flt3lg.S For: GACCTGCTCTCGTGCTTCTAT	Rev: GAGCAATGGGCATCTGGTTT
	flt3lg.L For: AAACCACATCCCCATTGCTCT	Rev: TTTCAGCACGACCGCTACTT
	znf366.L For: ATGGTCACCCTTCAAGTGCC	Rev: CATGCGAAGTTCTTTTGTGC
	baff.L For: TATGGGCAGGTTTGGTTCACA	Rev: ACCCACTTTCTGGGCCTTTTT
	ccl19.S For: AAACGCTACATCCGGCAAGA	Rev: GCTCGTGGGGAGGAATACAC
	IgM-C-DOM.L For: CCAGTTACTCCACTGGCCTC	Rev: CTTGGGAGCTGGCTGAGTAG
	spi1.S/L For: AGGCCATCAGGTCTCCTACA	Rev: CCCGAGAGTCCATCTCTCCA
	CD8a.S For: AAAGCGAGGAAAGGGTCGTT	Rev: GCTTTGTGGTCGTTGGCTTT
	CD8b.L For: GGAACACGTTTACCCTGAAGA	Rev: GGGAGGTTCCATTCCCAAAT
	CD3g.S For: TTGGGCTCAGTGTGGAATG	Rev: GGTCCCGGTATCCATCTCTA

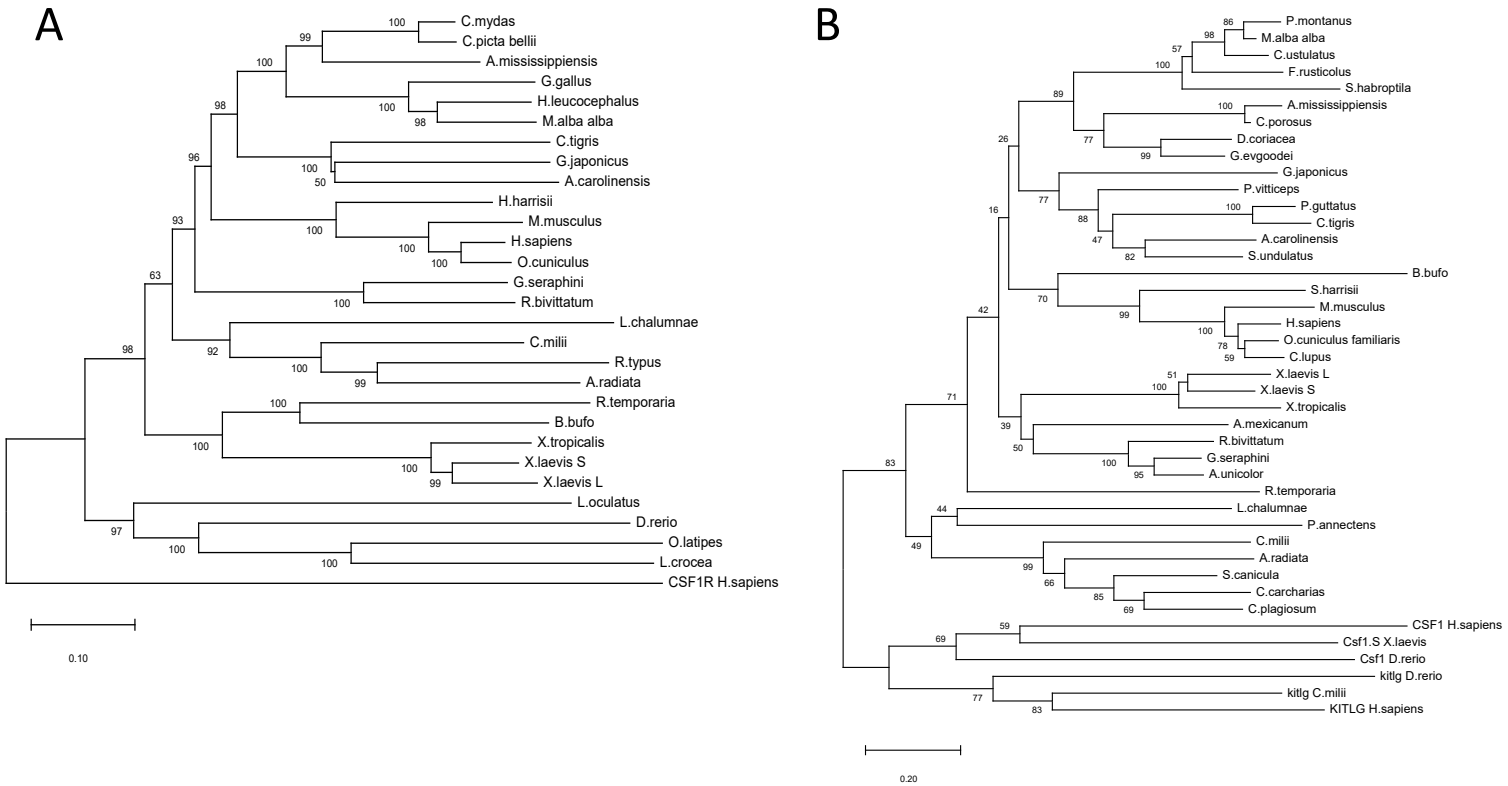

Fig. S1: Flt3 and Flt3lg phylogenetic tree obtained using the Neighbor-Joining method. The optimal trees are shown. The percentage of replicate trees in which the associated taxa clustered together in the bootstrap test (1000 replicates) are shown next to the branches (Felsenstein, 1985). The tree is drawn to scale, with branch lengths in the same units as those of the evolutionary distances used to infer the phylogenetic tree.

(A) Flt3 phylogenetic tree. Xenopus laevis_S: XP_041440445.1; Xenopus laevis_L: XP_041438590.1; Homo sapiens: P36888; Mus musculus: Q00342; Rana temporaria: XP_040196406.1; receptor-type Geotrypetes seraphini: XP_033804528.1; Bufo bufo: XP_040282105.1; Latimeria chalumnae: XP_014342109.1; Danio rerio: XP_021325994.1; Lepisosteus oculatus XP_015197226.1; Chelonia mydas: XP_037747523.1; Chrysemys picta bellii: XP_008165643.1; Gallus gallus, XP_003640660.3; Haliaeetus leucocephalus: XP_010571107.1; Rhincodon typus XP_020368760.1; Callorhinchus milii, XP_007898871.1; Amblyraja radiata: XP_032878726.1; Oryzias latipes: XP_023805694.1; Larimichthys crocea: XP_019129239.2; Alligator mississippiensis: XP_006270543.2; Sarcophilus harrisii: XP_031816610.1; Oryctolagus cuniculus XP_017192992.1; Rhinatrema bivittatum: XP_029458464.1; Gekko japonicus: XP_015260891.1; Anolis carolinensis: XP_008106152.1; Crotalus tigris: XP_039212794.1; Motacilla alba alba XP_038008564.1; Xenopus tropicalis: XP_012813386.2; CSF1 Homo sapiens: NP_001275634.1

(B) Flt3lg phylogenetic tree: Xenopus laevis_S: XP_018083675.1; Xenopus laevis_L:rna38573; Homo sapiens: P49771; Mus musculus: P49772; Alligator mississippiensis: XP_019344387.1; Xenopus tropicalis: XP_017951006.1; Strigops habroptila: XP_030330212.1; Sarcophilus harrisii: XP_031817621.1; Dermochelys coriacea: XP_038237782.1; Bufo bufo: XP_040288994.1; Rana temporaria: XP_040183561.1; Anolis carolinensis : XP_016852187.1; Gopherus evgoodei: XP_030400784.1; Oryctolagus cuniculus: XP_017195522.1; Passer montanus: XP_039582139.1; Canis lupus familiaris: NP_001003350.1; Motacilla alba alba : XP_037982352.1; Geotrypetes seraphini: XP_033815801.1; Rhinatrema bivittatum : XP_029441294.1; Pantherophis guttatus : XP_034279162.1; Gekko japonicus: XP_015274043.1; Crotalus tigris : XP_039191171.1; Rhinatrema bivittatum XP_029441293.1; Microcaecilia unicolor: XP_030053788.1; Crocodylus porosus : XP_019406541.1; Ambystoma mexicanum : AMEX60DD201016381.1; Callorhinchus milii : XP_007908029.1; Carcharodon carcharias : XP_041034055.1; Amblyraja radiata: XP_032869010.1; Scyliorhinus canicula: XP_038639819.1; Latimeria chalumnae : XP_014344282.1; Protopterus annectens : XP_043915747.1; Chiloscyllium plagiosum : XP_043535563.1; Crocodylus porosus : XP_019406541.1; Anolis carolinensis: XP_016852187.1; Microcaecilia unicolor : XP_030053787.1; Sceloporus undulatus: XP_042331912.1; Pogona vitticeps : XP_020648337.1; Catharus ustulatus : XP_032942611.1; Falco rusticolus : XP_037230781.1; CSF1 H. sapiens : XM_018247987.1; Kitlg D.rerio NP_001018133.1; Kitlg C. milii XP_007893508.1; Kitlg Homo sapiens : NP_003985.2; Csf1.S Xenopus laevis : NP_001267529.1

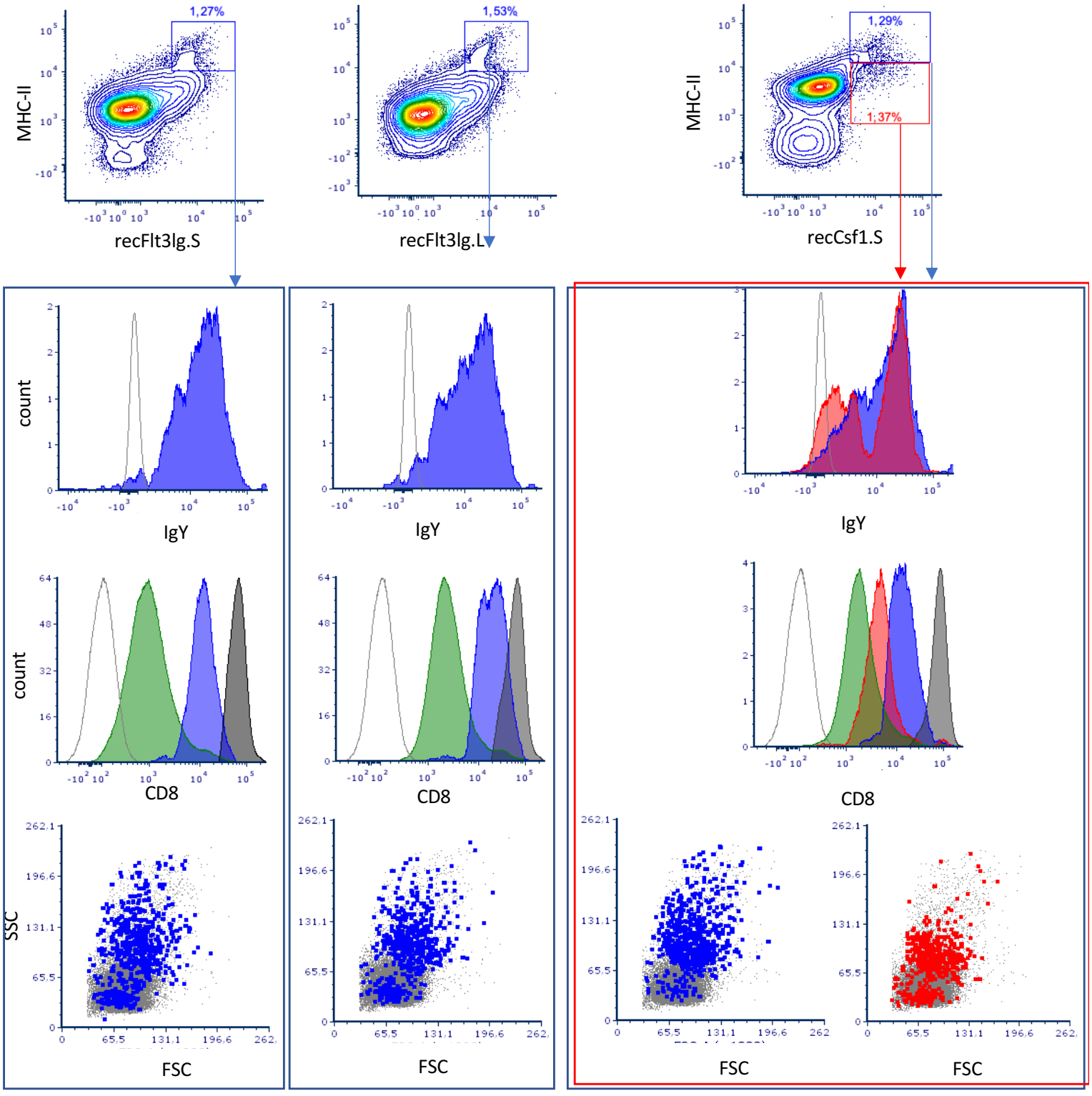

Fig. S2: Fig. S7: Characterization of recFlt3lg.S+, recFlt3lg.L+ and recCsf1+ XL cells by flow cytometry. XL cells were identified based on the high expression of MHC-II as described by Neely et coworker (2018). Gated MHC-II^{high+} recFlt3lg.S+, recFlt3lg.L+ and recCsf1.S+ XL cells and recCsf1.S+MHC-II+ macrophages were highlighted in blue and red respectively for IgY and CD8 staining as well as their size and complexicity (SSC and FSC). Histograms in white represents the isotype-matched control. The histograms correspond to the CD8 T cells.

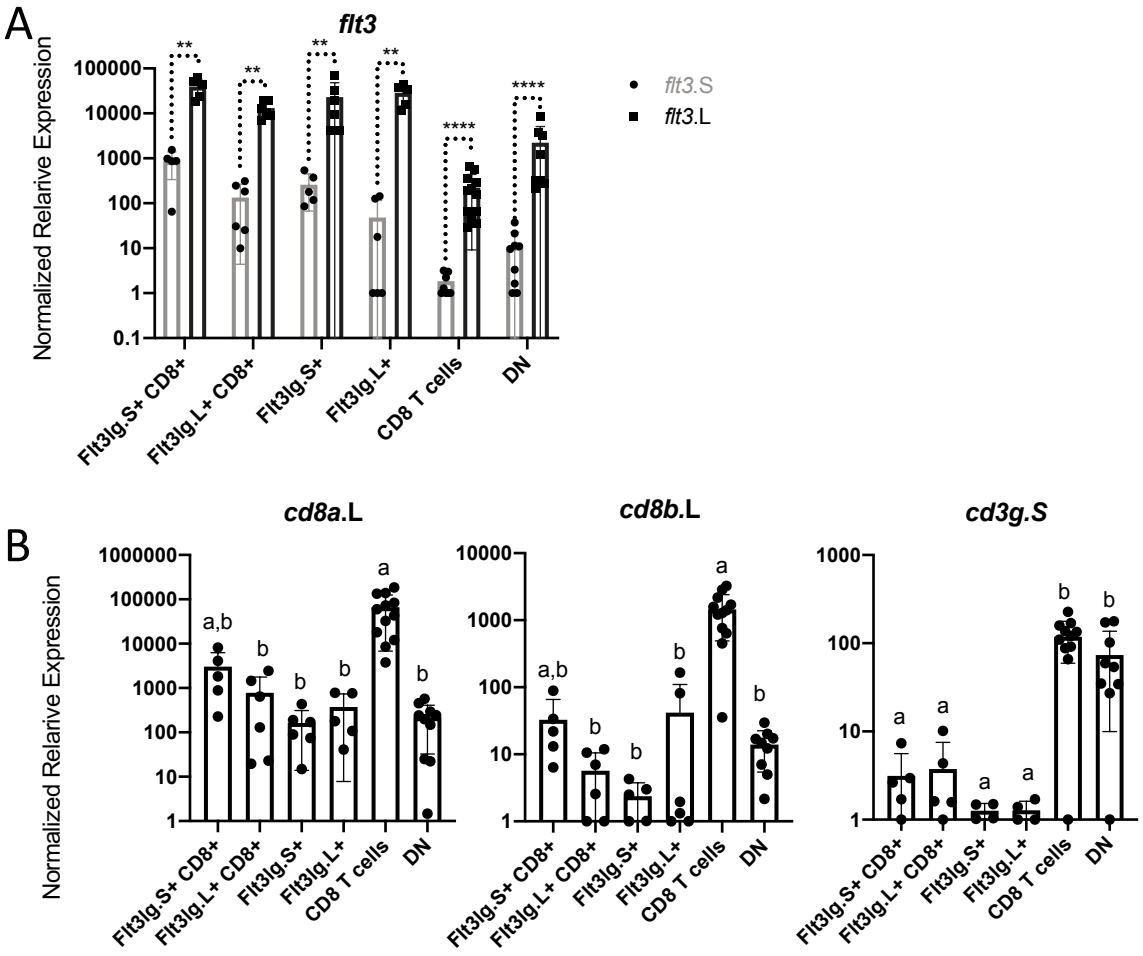

Fig. S3: RT-qPCR analysis of different splenocyte cell subsets sorted based on the recFlt3lg.S/L and CD8 staining. (A) Flt3 transcript levels in the different sorted subsets. ** and *** indicate statistical significance ($p<0.001$ and $p<0.0001$, respectively) between the flt3 homeologs using a Mann-Whitney test. (B) Relative expression of *cd8a*.L, *cd8b*.L and *cd3g*.S in the different sorted subsets. a-c indicate statistical significances differences between the experimental groups ($p<0.05$) using the non-parametric Kruskall-Wallis test followed by multiple step-up method of Benjamini, Krieger and Yekutieli), bars represent the mean with the standard deviation (n=6, two independent experiments).